International Journal of Nanoelectronics and Materials
Volume 15, No. 3, July 2022 [253-268]

Study of Transport Characteristics using Impedance Spectroscopy and Memristor Property Analysis of Protonated Polyaniline-WO_3 Nanocomposite

Jisha P[1*], Suma M S[2], Haneesh K M[3]

[1,2]Department of Medical Electronics Engineering, B.M.S. College of Engineering, Bangalore, India.
[3]Department of Electrical and Electronics Engineering, CHRIST University, Bangalore, India.

Received 14 February 2022, Revised 30 May 2022, Accepted 1 June 2022

ABSTRACT

Polyaniline-WO_3 nanocomposite was synthesized through in-situ chemical polymerization. The structural properties are studied by using XRD and FESEM characterization. The XRD results confirmed the presence of crystalline WO_3 nanoparticles in the polymer nanocomposite structure. FESEM images confirmed the sheet-like structure with heterojunction of WO_3 nanoparticles and polyaniline matrix. The transport properties of the synthesized nanocomposites are studied using impedance spectroscopy analysis. The complex impedance analysis conducted using the Nyquist plot and equivalent circuit model of the nanocomposites are simulated using ZSimpWin software. The major conduction mechanism in the material is found to be grain boundary effect and the grain boundary conduction parameters are calculated. The polyaniline-WO_3 nanocomposite with WO_3 doping concentration of 15% has exhibited better sensing characteristics towards the target VOC (Volatile Organic Compound) 3-Carene, a breath-based biomarker for malaria. The memristor sensor model of the polyaniline nanocomposite with 15% of WO_3 is simulated using MATLAB-Simulink. The pinched hysteresis loop obtained confirmed the memristor properties of the material.

Keywords: impedance analysis, memristor, polyaniline, WO_3, VOC sensor

1. INTRODUCTION

A memristor is considered to be a fourth fundamental element or a missed passive electronic component with many valuable circuit properties and it can be employed as a conceptual analysis tool [1]. The memristance naturally exists in nanoscale systems containing a conduction mechanism using electronic and ionic transport properties coupled together when an external bias voltage is applied and the results obtained have helped in explaining the voltage and current hysteresis behavior of many nanoscale systems. The first experimental realization of the memristor was using titanium dioxide thin-film layer with oxygen vacancies drift according to the applied electric field [2]. Metal oxide thin film layers are generally used for the construction of memristors. Yang et al. reported that the conduction mechanism in thin-film devices using metals or metal oxides is based on the spatially heterogeneous electronic barrier [3]. Many works have been reported recently on memristors using different types of materials including metal oxides, chalcogenides, and polymers [4]. The resistive switching properties and the operation approaches in nanoscale memristance devices are acquiring more research importance due to their vast application. Organic memristors are also gaining more attention in the present research scenario. The properties and structure of an organic memristor using a thin film of conducting polymer material like polyaniline with channel thickness in mm range was reported by Erokhin et al. [5]. The results have shown that the addition of metal oxide nanoparticles can yield better electrical properties through the Schottky effect or single electron phenomena. The conducting

*Corresponding author: jishap.ml@bmsce.ac.in

polymer-based memristor systems use reversible electrochemical redox reactions as the working principle with different conductivity ranges indicating ON and OFF states using different resistance values [6]. Nowadays, metal oxide-based nanoscale devices for gas sensing applications are gaining more popularity due to their miniaturized size and low power consumption [7]. The resistive switching properties of memristors have been investigated widely for their use as a sensing element in nano devices with biosensing applications [8]. A memristor-based hydrogen sensor using Pt/TiO_2/Pt material at room temperature was reported [9]. On exposure to the target gas, the resistance will vary depending on the material used. The adsorption of the target gases can alter the equilibrium of charge carriers present in the sensing material.

While exposed to the reducing type of gases the resistance is found to be increasing in P-type semiconductor materials, resistance decreases for N-type semiconductor sensing layers. The exposure oxidizing gases will decrease the resistance of P-type semiconductors and increase the resistance in N-type semiconductor material [10]. An Ag/TiO_2/Cu thick film radiation memristor sensor with low power consumption and reduced sensing area was also reported [11]. Nafion based memristor integrated with a piezo resistive pressure sensor was demonstrated and it was able to read and process a pressure stimuli using a set of amplitude or frequency [12]. The memristive switching characteristics of Cu/ HfO_2/p++ Si device made using a polymer assisted spin coating method was studied and its memristive sensing properties for gamma-ray detection were analyzed [13]. Researchers are focused on polyaniline based memristors due to the ease of processing and biocompatibility. The active channel dimension reduction can aid in achieving a high switching rate in polyaniline based memristive devices [14]. Recently, conductive filler containing polymer nanocomposites are gaining significant research interest due to their edge effect properties suitable for memristor applications. A polymer nanocomposite using graphene oxide as filler was reported and write-once-read-many-times (WORM) characteristic was studied by varying thickness of the active layer and filler doping concentration to propose a conduction mechanism [15]. A polymer nanocomposite synthesized using polyaniline and gold nanoparticles was used to fabricate a memristive device to study the Schottky barrier threshold-based conduction mechanism [16]. Resistive switching behavior of the WO_3 active layer prepared using the spray pyrolysis method with the Ag electrode in a thin film memristor device was reported [17]. A study on the memristive material properties has shown that memristors exhibit bipolar and unipolar resistive switching characteristics [18].

A memristor will always have a pinched hysteresis loop when driven by a periodic voltage or current source without any DC component, as magnetic flux developed with the passage of charges. The resistance variation in the memristor can be recorded to indicate the presence of the gas to be detected and this can be modeled as a memristor sensor. When the memristor is exposed to a particular gas concentration, the resistance variation occurs depending on the sensing material used. So, modeling these characteristics of a sensor is the main block in a smart sensing system design. Using different structural models of the sensing system and modeling the response and recovery behavior, the performance of a smart sensing system can be evaluated. The model discussed in this work can be used to model the initial blocks of a smart sensing system for the simulation of the complete system behavior. The occurrence of system runtime errors can be identified before implementing the actual system. So, if the errors are detected earlier then the time and cost needed to solve these issues can be saved. The internal structure of the sensor element is shown in Figure 1, where the polyaniline-WO_3 nanocomposite is coated on an alumina substrate and two electrodes are attached to the substrate. On exposure to the target VOC, the 3-Carene molecules got trapped on the porous surface of the sensing material, hence the conductivity of the sensor decreases. The thickness of the effective sensing area varies concerning the concentration of target VOC 3-Carene is marked as W in Figure 1, and the total thickness of the sensor element is considered as D.

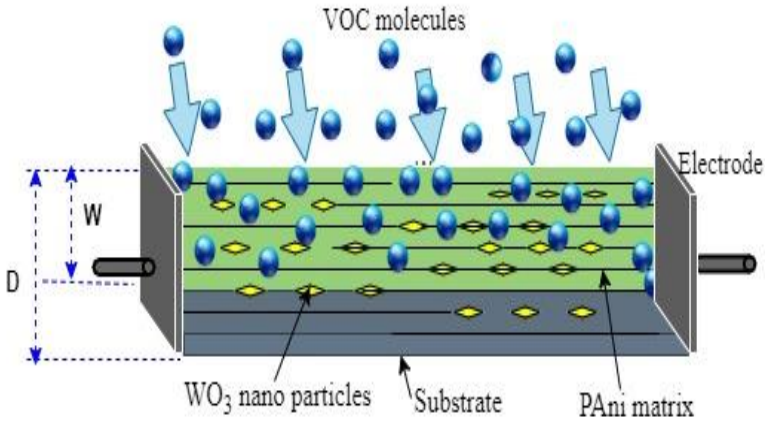

Figure 1. Structure of the sensor when exposed to VOC molecules

This work aims to study the conduction mechanism inside the polyaniline-WO_3 nanocomposite and to analyze the memristive properties. The drop cast memristor sensor is non-linear in nature and its transport mechanisms are correlated to each other. Polyaniline-WO_3 nanocomposite is synthesized through in-situ chemical polymerization and drop casted on an alumina substrate attached with copper electrodes to study the VOC sensing characteristics. PVDF (polyvinylidene difluoride) has been used as a binding agent to get good adhesion of the nanocomposite on the substrate. The conductivity studies have been made through impedance analysis using ZSimpWin software to study the major conduction mechanism in the polymer nanocomposite. Also, the memristor properties of the synthesized nanocomposite for VOC sensing application have been studied using MATLAB-Simulink simulations. The results confirmed memristive properties of the polyaniline-WO_3 nanocomposite and this can be used as a foundation for the memristive VOC sensor-based system development.

2. MATERIAL AND METHODS

2.1 Materials

Aniline monomer, WO_3 nanoparticles, ammonium persulphate as oxidizing agent for polymerization, and the binding material PVDF were procured from Sigma Aldrich. The in-situ chemical polymerization of aniline monomer was done in concentrated HNO_3 acid-based acidic medium to get the protonated emeraldine salt form of the polyaniline matrix. N-Methyl-2-Pyrrolidone (NMP) was purchased from Sigma Aldrich and it is used for coating polyaniline-PVDF nanocomposite mixture on an alumina substrate. All solutions were prepared using double distilled water. All reagents were used without any additional purification. The VOC used for sensing application, 3-Carene, was procured from TCI Chemicals (India) Pvt. Ltd. Emeraldine salt form of polyaniline nanocomposites using WO_3 nanoparticles of different concentrations were synthesized through in-situ chemical polymerization. The powdered form of polyaniline nanocomposite is mixed with PVDF in 1:5 ratio and N-Methyl-2-Pyrrolidone (NMP) is added to this mixture. The polyaniline nanocomposite is drop casted on alumina substrate attached with copper electrodes and dried in a hot air oven at 60^0C to make the sensor prototypes.

2.2 Characterizations of the Nanocomposite

The structural characterization for the determination of phase and crystal structures in the nanocomposites was carried out by the powder method of X-ray diffraction on the XPERT-3 diffractometer with λ=1.54060 Å and 2θ range from 10 to 80^0 with a size of 0.03 steps per 0.8 s. The impedance measurement at room temperature, for frequencies 100 Hz to 5 MHz, of the synthesized WO_3 embedded polyaniline nanocomposite was done using Wyne Kerr 6500B Precision Impedance Analyzer. 13mm diameter pellets prepared by using hydraulic press were

used for this study. Silver paste coated pellets were placed between the probes of impedance analyzer instrument to measure impedance phase angle, conductance, capacitance, and dissipation factor. The measured impedance values were used to plot the cole-cole plot for the complex impedance analysis to find the conduction mechanism inside the polyaniline-WO_3 nanocomposite. The morphology of the polyaniline nanocomposite synthesized with 15% doping concentration was investigated by using FESEM (Field Emission Scanning Electron Microscope). VOC sensing studies were carried out in a specially designed glass chamber by using a 6 ½ digit digital multimeter. The measured resistance values were used to study the gas sensing memristor characteristics of the polyaniline-WO_3 nanocomposite using MATLAB simulation.

3. RESULTS AND DISCUSSION

3.1 X-Ray Diffraction Studies

The crystalline phase formation in the polyaniline nanocomposite due to the addition of WO_3, in different weight percentages of 5%, 10%, 15%, and 20%, were studied by X-ray diffractogram (XRD) with 2θ in the range of 10 to 80^0 as shown in Figure 2. The polycrystalline nature of WO_3 nanoparticles were observed in the XRD pattern with a monoclinic crystal structure (ICDD DATA CARD 98-001-5905). The most significant diffraction peaks in the nanocomposites were corresponding to (100), (020), (002), (02-1), (111), (120), (02-2), (10-2), (12-2), (004), (211) and (12-4) crystal planes. The crystalline and amorphous characteristics together made the material more conductive and suitable for VOC sensing. The average crystallite size of WO_3 embedded polyaniline nanocomposite was calculated by using Debye-Scherer's formula [19]:

$$D = \frac{K\lambda}{\beta \cos\theta} \tag{1}$$

where K =0.94, λ is wavelength of X-ray, β is the full width half maximum of the diffraction peaks in Radians and θ is the diffraction angle. The average crystallite size of the polyaniline-WO_3 nanocomposites with 5%, 10%, 15%, and 20% weight percentages of WO_3 nanoparticles were calculated and found to be nearly 18 nm, 19 nm, 20 nm, and 21 nm respectively. The emeraldine salt form of polyaniline synthesized in nitric acid medium shows higher values of strain, dislocation density, d-spacing, and interchain separation compared to polyaniline-WO_3 nanocomposite [20]. Also, inter chain separation length was found to be decreasing when the WO_3 doping concentration increased. The parameters calculated from the XRD diffractogram of the synthesized polyaniline nanocomposites with different doping concentrations of WO_3 nanoparticles is mentioned in Table 1.

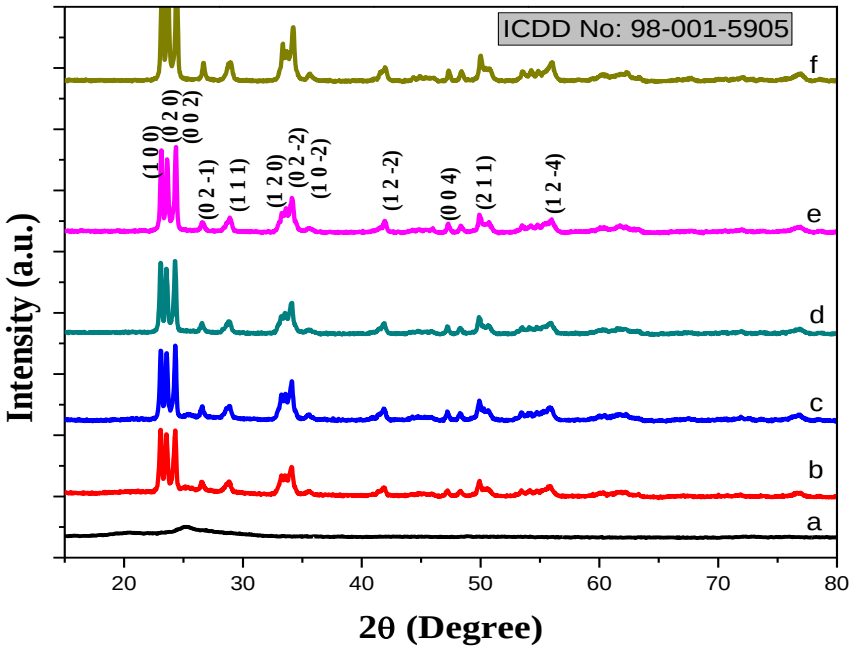

Figure 2. XRD patterns of: a) HNO_3 acid protonated PAni, b) PAni - HNO_3 / WO_3 -5%, c) PAni - HNO_3 / WO_3 -10%, d) PAni - HNO_3/ WO_3 -15%, e) PAni - HNO_3 / WO_3 -20%, f) WO_3 nanoparticles

Table 1. The XRD parameters calculated for the synthesized polyaniline nanocomposites

Materials	Average crystallite size, D (nm)	Average interchain separation length, R (A^0)
PAni- HNO3	1.59	0.5005
PAni - HNO_3/WO_3 5%	18.53	0.2876
PAni - HNO_3/WO_3 10%	18.76	0.2838
PAni - HNO_3/WO_3 15%	20.44	0.2810
PAni - HNO_3/WO_3 20%	20.63	0.2809

3.2 Impedance Analysis

The impedance analysis for the electrical characterization of the synthesized polyaniline -WO_3 nanocomposite was done by complex impedance spectroscopy method using cole-cole (Nyquist) plots, to understand the complete conduction mechanism and relaxation methods [21]. The dielectric relaxation mechanism due to bulk or grain boundary effect can be understood by using a bricklayer model was the bulk type conduction is represented by RC elements connected in parallel [22]. Similarly, the series events of bulk type conduction will be represented by the series connection of these RC parallel units, where the capacitor represents the charge storage ability and leakage current caused by the un-trapped charges are represented by the resistor element. Complex plane impedance analysis using the Nyquist plot method is generally used for the polymer nanocomposites, which yields semicircles based on the number of parallel RC circuits obtained for the material used. Depending on the position of semicircle obtained in the Nyquist plot, the conduction mechanism behind the nanocomposite can be concluded. The bulk (grain) conduction effect is represented by semicircle at the high-frequency region and the semicircle at the low-frequency region of the Nyquist plot represents the contribution of polymer electrodes.

The semicircle at the intermediate frequency region corresponds to the grain boundary effect in the conduction mechanism [23].

To study the transport properties of the synthesized polyaniline-WO_3 nanocomposite, impedance of each material for a frequency variation from 100Hz to 5MHz at room temperature was measured using Precision Impedance Analyzer. The impedance analysis of the synthesized polyaniline-WO_3 nanocomposite was done using ZSimpWin software of Version-3.21 to derive the equivalent circuit model. The complex impedance analysis using the Nyquist plot for the HNO_3 acid doped polyaniline matrix is shown in Figure 3. The depressed semicircle nature at the intermediate frequency range of the Nyquist plot shows that the major conduction mechanism behind the synthesized polymer matrix is grain boundary effect [24]. Also, the small bending in the high-frequency range contributes to the slight amount of bulk conduction in the material. Hence the simulated equivalent circuit as shown in Figure 3 consists of a series resistance (R1) with a parallel RC element (R2 parallel with C1) and a parallel circuit of a resistor (R3) with a constant phase element (CPE1) to represent the dielectric properties. The impedance response of the constant phase element (CPE) can be calculated by using the following equation [25]:

$$\hat{Z}_{CPE} = \frac{1}{Q \times (j\omega)^n} \tag{2}$$

where the value of the exponent parameter 'n' will be in the range of -1 to 1 and the pre-factor Q has properties similar to capacitor since the 'n' value is close 1 in this case of HNO_3 acid doped polyaniline matrix. From the simulation results, the obtained 'n' value for this material is 0.9035. When the value of 'n' is equal to zero the Z_{CPE} represents the impedance of a resistor, while constant phase element factor Q will be numerically equal to the reciprocal of its resistance and value of 'n' close to -1 indicates Z_{CPE} as the approximated impedance due to an inductor [26].

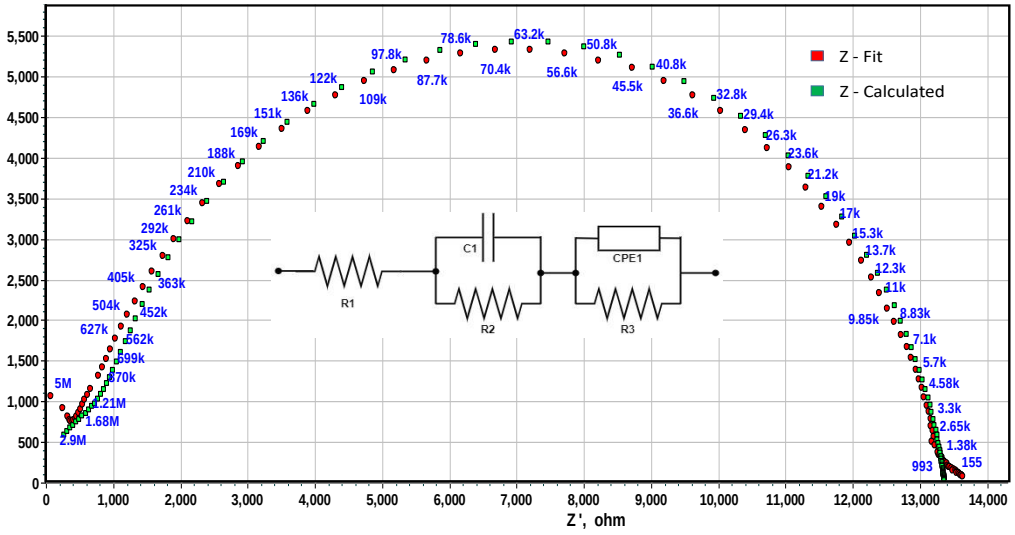

Figure 3. Complex plane Nyquist plot of HNO_3 doped polyaniline with its equivalent circuit

The total impedance of the equivalent circuit obtained for the HNO_3 acid doped polyaniline is given by:

$$\hat{Z} = R_1 + \left(\frac{1}{R_2} + j\omega C_1\right)^{-1} + \left(\frac{1}{R_3} + \frac{1}{\hat{Z}_{CPE1}}\right)^{-1} \tag{3}$$

Substituting for the impedance of CPE1 as $\frac{1}{\hat{Z}_{CPE}} = Q \times (j\omega)^n$ and separating the real and imaginary parts of the impedance equation, we get:

$$Z^{'} = R_1 + \frac{R_2}{1+\omega^2 C_1^2 R_2^2} + \frac{R_3(1+RQ_{CPE1}\omega^n \cos(\frac{n\pi}{2}))}{1+2R_3 Q_{CPE1}\omega^n \cos(\frac{n\pi}{2}) + (R_3 Q_{CPE1}\omega^n)^2} \quad (4)$$

$$Z^{''} = -\frac{\omega C_1 R_2^2}{1+\omega^2 C_1^2 R_2^2} + \frac{R_3^2 Q_{CPE1}\omega^n \sin(\frac{n\pi}{2})}{1+2R_3 Q_{CPE1}\omega^n \cos(\frac{n\pi}{2}) + (R_3 Q_{CPE1}\omega^n)^2} \quad (5)$$

where $Z^{'}$ is the real part of the impedance equation and $Z^{''}$ represents the imaginary part. Curve fitting using Equations (3) and (4) to the Nyquist plot of HNO_3 doped polyaniline material is shown in Figure 3. The equivalent parameters obtained for the fit are shown in Table 2.

The complex impedance analysis using the Nyquist plot for the polyaniline-WO_3 nanocomposites are shown in Figure 4. The depressed semicircle nature similar to the HNO_3 doped polyaniline matrix at the intermediate frequency range of the Nyquist plot shows that the major conduction mechanism behind the synthesized polyaniline-WO_3 nanocomposites are grain boundary effect. The small extension in the high-frequency range for 5%, 10%, and 20% weight concentration of WO_3 contribute to the slight amount of bulk conduction inside the nanocomposite. Hence the simulated equivalent circuit consists of a series resistive element with a parallel RC element and a parallel circuit of a resistor with a constant phase element to represent the dielectric properties. The polyaniline-WO_3 nanocomposite with a doping concentration of 5% has an equivalent circuit consisting of three parallel elements including a constant phase element (CPE1), a resistive element (R1) and a resistance (R2) in series with a constant phase element (CPE2). The total impedance of the equivalent circuit obtained through impedance spectroscopy simulation of polyaniline- WO_3 nanocomposites with a doping concentration of 5% is given by:

$$\hat{Z} = \left(\frac{1}{\hat{Z}_{CPE1}} + \frac{1}{R_1} + \frac{1}{R_2 + \hat{Z}_{CPE2}} \right)^{-1} \quad (6)$$

Curve fitting using the equations of real and imaginary parts of the total impedance, obtained by substituting impedance of CPE elements, with the Nyquist plot yields the exponent parameter for CPE1 of the equivalent circuit is equal to 1, which indicates that it is a pure capacitive element. For the second constant phase element (CPE2) in the circuit, the exponent parameter 'n' has a value of 0.8784 which is nearly equal to one, and hence it has properties similar to a capacitive element. The non-uniformity of the material surface or chemical inhomogeneity of the doping agent can cause the deviation of the 'n' value from unity [27]. The equivalent circuit of polyaniline-WO_3 nanocomposite with 10% doping concentration consists of three circuit blocks connected in series. The first block is a parallel combination of CPE1, R1, and R2 connected in series with CPE2. The second circuit block is a parallel circuit of R3 and CPE3 and the third part of the equivalent circuit is a constant phase element (CPE4) connected in series. The total impedance of the equivalent circuit obtained for polyaniline-WO_3 nanocomposite with a doping concentration of 10% is given by:

$$\hat{Z} = \left(\frac{1}{\hat{Z}_{CPE1}} + \frac{1}{R_1} + \frac{1}{R_2 + \hat{Z}_{CPE2}} \right)^{-1} + (\frac{1}{R_3} + \frac{1}{\hat{Z}_{CPE3}})^{-1} + \hat{Z}_{CPE3} \quad (7)$$

Curve fitting using the equations of real and imaginary parts of the total impedance with the Nyquist plot of polyaniline-WO_3 nanocomposites with a doping concentration of 10% yields the exponent parameter 'n' for CPE1 and CPE3 as unity and it indicates that these are pure capacitive elements. The 'n' value for CPE2 is obtained as 0.5454 and it indicates that CPE2 is a Warburg element, which confirms the modeling of the semi-infinite linear diffusion [26]. Also, the exponent parameter 'n' for CPE4 is found to be 0.212, since the value is near to zero this element is an

admittance element with properties close to a resistor. All the equivalent circuit parameters obtained for the curve fit are listed in Table 2. The equivalent circuit of polyaniline-WO_3 nanocomposite with 15% doping concentration consists of three resistors and constant phase element circuit blocks connected in series. Each block is a parallel combination of resistance element (R) and a constant phase element (CPE). The total impedance of the equivalent circuit obtained for polyaniline-WO_3 nanocomposites with a doping concentration of 15% is given by:

$$\hat{Z} = \left(\frac{1}{R_1} + \frac{1}{\hat{Z}_{CPE1}}\right)^{-1} + \left(\frac{1}{R_2} + \frac{1}{\hat{Z}_{CPE2}}\right)^{-1} + \left(\frac{1}{R_3} + \frac{1}{\hat{Z}_{CPE3}}\right)^{-1} \tag{8}$$

Curve fitting using the equations of real and imaginary parts of the total impedance calculated using Equation (7) with the Nyquist plot of polyaniline-WO_3 nanocomposites with a doping concentration of 15% yields the exponent parameter 'n' for CPE1, CPE2 and CPE3 close to unity and it indicates that these are pure capacitive elements. The 'n' value for CPE1 is obtained as 0.9904, 'n' value for CPE2 is found to be 0.9387 and for CPE3 the 'n' value is unity, since the value is very close to unity these elements will behave like pure capacitors.

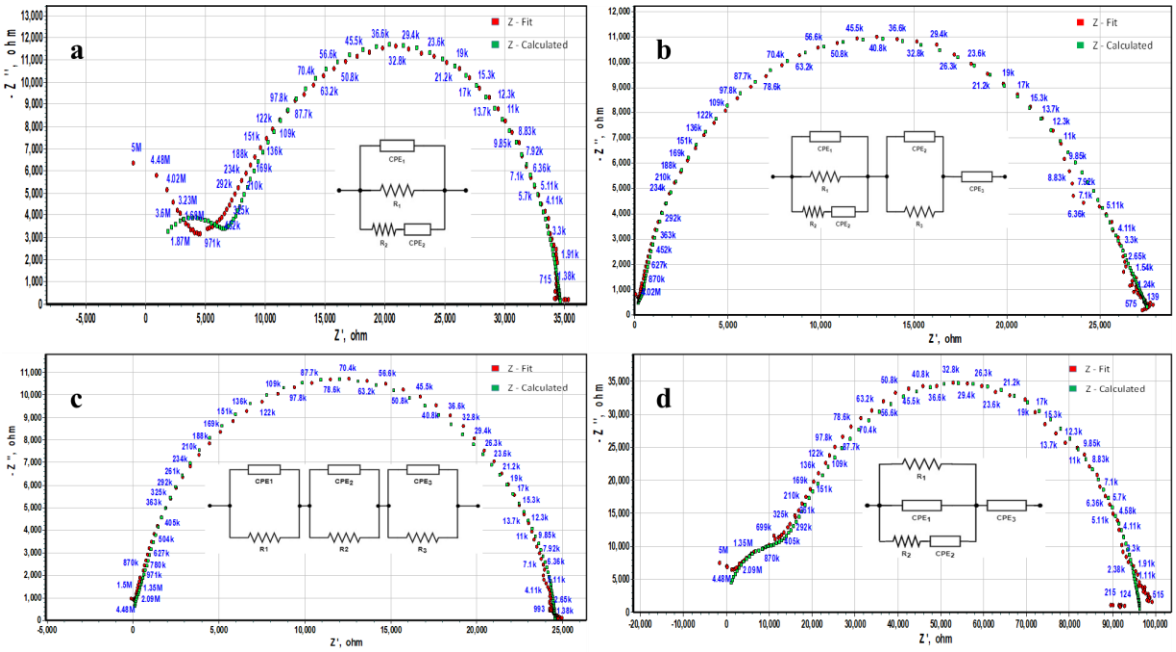

Figure 4. Complex plane Nyquist plot of polyaniline-WO_3 with its equivalent circuit: a) PAni - HNO_3 / WO_3 -5%, b) PAni - HNO_3 / WO_3 -10%, c) PAni - HNO_3/ WO_3 -15%, d) PAni - HNO_3 / WO_3 -20%

WO_3 doped polyaniline nanocomposite with 20% doping concentration contains an equivalent circuit of resistors and constant phase elements parallel network in series with another constant phase element. The circuit is quite similar to the equivalent circuit of 10% doping concentration WO_3-polyaniline nanocomposite. The total impedance of the equivalent circuit obtained for WO_3 doped polyaniline nanocomposites with a doping concentration of 20% is given by:

$$\hat{Z} = \left(\frac{1}{R_1} + \frac{1}{\hat{Z}_{CPE1}} + \frac{1}{R_2 + \hat{Z}_{CPE2}}\right)^{-1} + \hat{Z}_{CPE3} \tag{9}$$

Curve fitting using the equations of real and imaginary parts of the total impedance with the Nyquist plot of polyaniline-WO_3 nanocomposites with a doping concentration of 20% yields the exponent parameter 'n' for CPE1 as unity and it indicates that this is a pure capacitive element. The exponent parameter 'n' for CPE2 is found to be 0.8683, since the value is near to unity this element will also behave like a capacitor. The 'n' value for CPE3 is obtained as 0.6366 and it indicates that CPE3 is almost similar to the Warburg element, which confirms the semi-infinite

linear diffusion inside the material [26]. All the equivalent circuit parameters obtained for the curve fits are listed in Table 2.

The depressed semicircle Nyquist plot of the polyaniline-WO_3 nanocomposite shows that the material obeys a non-Debye model of relaxation mechanism. The mean relaxation time of grain and grain boundary conduction processes are denoted by τ_g and τ_{gb} respectively.

Table 2. Equivalent circuit parameters obtained through complex impedance analysis simulation and curve fitting

Material	Equivalent Circuit Parameter values		
	Resistance	Capacitance/Constant Phase element	n - Value
PAni- HNO_3	R1 = 0.026 Ω	C1 = 6.623 x 10^{-11} F	n = 0.9035
	R2 = 735.8 Ω	CPE 1 = 6.412 x 10^{-10} Ω^{-1}	
	R3 = 1.263 x 10^4 Ω		
PAni - HNO_3/WO_3 5%	R1 = 3.47 x 10^4 Ω	CPE 1 = 7.109 x 10^{-12} Ω^{-1}	n_1 = 1
	R2 = 9723 Ω	CPE 2 = 4.384x 10^{-10} Ω^{-1}	n_2 = 0.8784
PAni - HNO_3/WO_3 10%	R1 = 2.73 x 10^4 Ω	CPE 1 = 1.207 x 10^{-10} Ω^{-1}	n_1 = 1
	R2 = 1.579 x 10^4 Ω	CPE 2 = 1.471x 10^{-8} Ω^{-1}	n_2 = 0.5454
	R3 = 492 Ω	CPE 3 = 9.065 x 10^{-11} Ω^{-1}	n_3 = 1
		CPE 4 = 9.618x 10^4 Ω^{-1}	n_4 = 0.212
PAni - HNO_3/WO_3 15%	R1 = 1.914 x 10^4 Ω	CPE 1 = 1.055x 10^{-10} Ω^{-1}	n_1 = 0.9904
	R2 = 4748 Ω	CPE 2 = 2.916x 10^{-9} Ω^{-1}	n_2 = 0.9387
	R3 = 671.2 Ω	CPE 3 = 1.471x 10^{-10} Ω^{-1}	n_3 = 1
PAni - HNO_3/WO_3 20%	R1 = 9.647 x 10^4 Ω	CPE 1 = 6.552x 10^{-12} Ω^{-1}	n_1 = 1
	R2 = 2.198 x 10^4 Ω	CPE 2 = 1.929x 10^{-10} Ω^{-1}	n_2 = 0.8683
		CPE 3 = 24.27 Ω^{-1}	n_3 = 0.6366

The relaxation time is the inverse of peak frequency, ω of the impedance curve in the Nyquist plot. So the relaxation time for grain and grain boundary can be expressed as, $\tau_g = \frac{1}{\omega_g} = R_g C_g$ and $\tau_{gb} = \frac{1}{\omega_{gb}} = R_{gb} C_{gb}$, where R_g and R_{gb} are the resistance contributed by the grain and grain boundaries, C_g and C_{gb} are the computed grain capacitance and grain boundary capacitance of the material. The DC resistance due to grain boundary effect can be computed from the Nyquist

plot by finding the intercept of the curve at the low-frequency region of the real axis and the DC conductivity can be calculated using this data. The specific grain boundary conductivity of the material can be calculated from the impedance analysis curve using the following equation:

$$\sigma_{sgb} = \sigma_{gb} \times \frac{d}{D} \tag{10}$$

where σ_{gb} is the gain boundary conductivity, D is the grain size of the material and d is the grain boundary thickness. The average grain boundary thickness is taken as ~1nm. So, increased grain size will affect the specific grain conductivity inversely. The grain boundary conductivity is calculated using grain boundary resistance value measured from the Nyquist plot (R_{gb}) along with thickness and area of the pellets used for the impedance measurement using the impedance analyzer. The dielectric constant of the material can be calculated by using specific grain boundary capacitance C_{sgb} and it is related to the grain boundary capacitance by the equation:

$$C_{sgb} = C_{gb} \times \frac{1}{D} \tag{11}$$

where C_{gb} is the grain boundary capacitance, D is the grain size and l is the thickness of the sample [28]. The calculated values of the specific parameters for the grain boundary region of the polyaniline-WO_3 nanocomposites are listed in Table 3.

Table. 3 The specific parameters for the grain boundary region of the polyaniline-WO_3 nanocomposites

Parameters	PAni-HNO_3	PAni - HNO_3/WO_3 5%	PAni - HNO_3/WO_3 10%	PAni - HNO_3/WO_3 15%	PAni - HNO_3/ WO_3 20%
R_{gb} (kΩ)	13.27	31.65	26.99	24.61	96.831
σ_{gb} (10^{-3} $\Omega^{-1}m^{-1}$)	0.625	0.262	0.307	0.306	0.0778
σ_{sgb} (10^{-3} $\Omega^{-1}m^{-1}$)	0.393	0.0141	0.0164	0.0150	0.0038
C_{gb} (nF)	1.19	0.963	0.908	0.577	0.315
C_{sgb} (μF)	825	57.2	53.2	28.2	15.3
ϵ_{gb}	703	48.7	45.4	24.1	13

3.3 Analysis of Memristor Sensor Properties

Figure 5 shows the FESEM (Field Emission Scanning Electron Microscope) image of polyaniline-WO_3 nanocomposite with 15% doping concentration and it confirms the sheet-like structure of polyaniline nanocomposite with non-uniformly distributed WO_3 nanoparticles above and below the sheet structure. The sheet-type structure of the matrix provides more surface and a porous structure which helps in achieving good sensitivity [29]. The n-type WO_3 particles and p-type polyaniline matrix together form heterojunction structures and hence this sample exhibited better conductivity and good sensing characteristics [30].

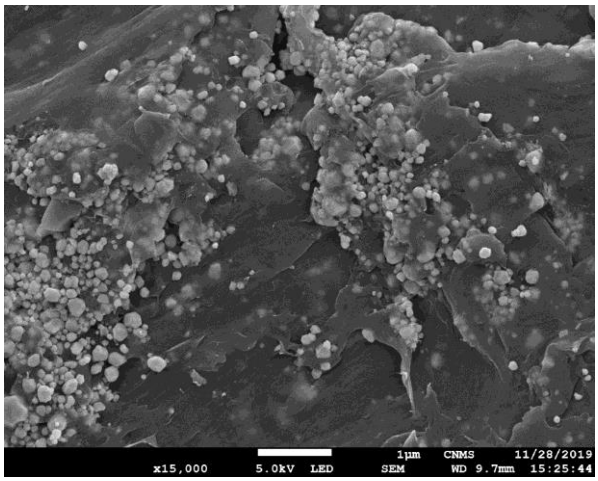

Figure 5. FESEM image of polyaniline-WO_3 nanocomposite with a doping concentration of 15%

The mathematical relation for a memristor can be expressed as:

$$M(q) = \frac{d\varphi}{dq} \tag{12}$$

where $M(q)$ is the memristance of the element which varies with the charge q passing through it and φ is the magnetic flux associated with it [31].

In a memristor sensor, the difference in target VOC concentration gives the resistance change. The voltage $v(t)$ at any instant t, across the element, is given by:

$$v(t) = R_m(x)i(t) \tag{13}$$

where R_m is the total resistance of the memristor, $x = \frac{W}{D}$, which is the relative depth of VOC penetration in *nanometer* and $i(t)$ is the current through the element. The thickness of the effective sensing area varies concerning the concentration of target VOC, 3-Carene is considered as *W* and the total thickness of the sensor element is considered as *D.* The rate of change of state x depends on the current passing through the memristor and is given by:

$$\frac{dx}{dt} = kf(x)i(t) \tag{14}$$

where, $k = \frac{\mu_v R_{on}}{D^2}$, dopant mobility $\mu_v = 10^{-14} m^2 s^{-1} V^{-1}$, R_{off} is the element resistance with $W = 0$ and R_{on} is the resistance with gas on.

The total memristor resistance can be expressed as:

$$R_m = R_{on}x + R_{off}(1-x) \tag{15}$$

The window function $f(x)$ is used to model the charge movement within the nanocomposite. There are many functions to model the window functions, but the Joglekar's window function offers a better nonlinear model, which has been used in this work [32]. The Joglekar's window function is given by:

$$f(x) = 1-(2x-1)^{2P} \tag{16}$$

where, P is a positive integer which controls the linearity of the model, here P is taken as 10. Using Equations (13)-(16), memristor model of the sensing element can be realized. To simulate the behavior of the sensing element, a model developed by using these equations on MATLAB-Simulink. Simulations were done for 5 sec, by applying a constant current source of 1 micro Ampere with a frequency of 5 rad/s. R_{on} is taken as 36KΩ and R_{off} as 25 KΩ based on the resistance values obtained in the sensing studies conducted. The voltage waveform obtained when the alternating current applied to the sensing element is shown in Figure 6.

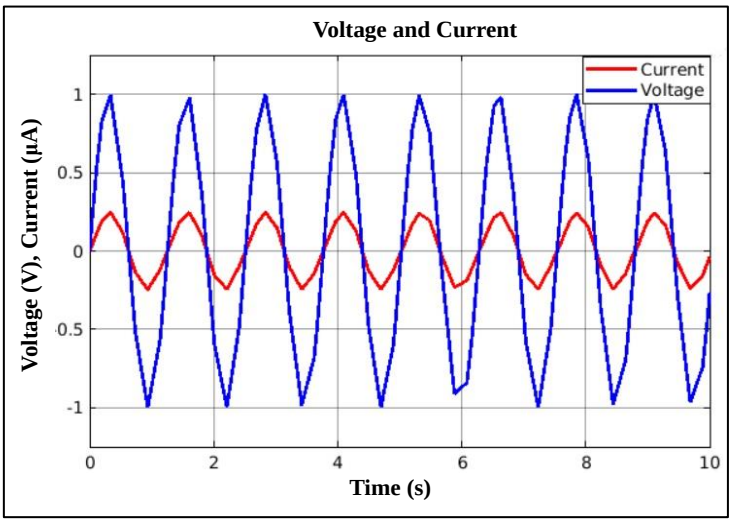

Figure 6. Voltage-Current waveforms in the sensing element

It was observed that the voltage and current differ only in magnitude and there is no phase difference observed like in the case of an inductor or a capacitor, so the nanocomposite exhibits resistance like behavior as in the case of any memristor element. The current and voltage waveforms cross zero at the same instant and it indicates the passive nature of the nanocomposite under test, so no energy storage is happening in the sensing element.

The charge–flux variations of the important measure of a memristor element and from the charge-flux curve obtained from the simulations are shown in Figure 7 and the slope of the curve is the measure of memristance of the sensor as mentioned in Equation (12). The positive slope of the charge-flux curve indicates a positive memristor and thus the passive behavior of the element. A capacitor will usually store energy in the form of an electric field and an inductor will store energy in the form of a magnetic field, but here the charge-flux curve is passing through the origin, which indicates that there is no energy storage in the element like a capacitor or an inductor. So, from the voltage-current waveforms and the charge-flux curves, it can be seen that the material is showing memristance properties.

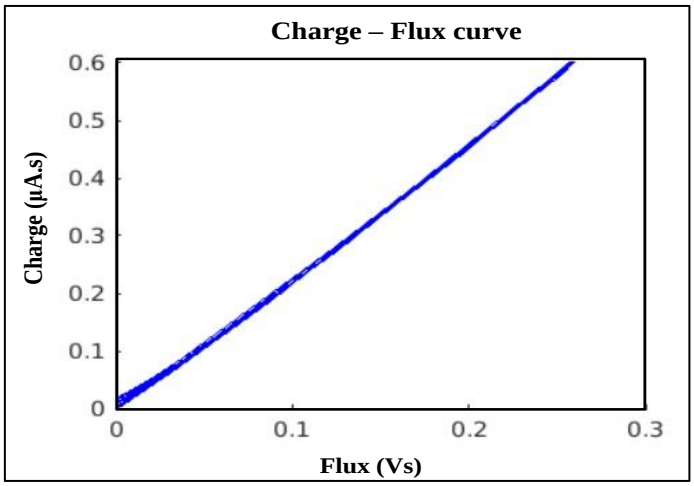

Figure 7. Charge-Flux curve of the sensing element

The hysteresis loop of the sensing element obtained through the simulations is shown in Figure 8. The simulation study was conducted only for 3ppm concentration of 3-Carene exposure on polyaniline-WO_3 nanocomposite with a doping concentration of 15%. The loop was obtained by plotting the voltage across the element for different current magnitudes.

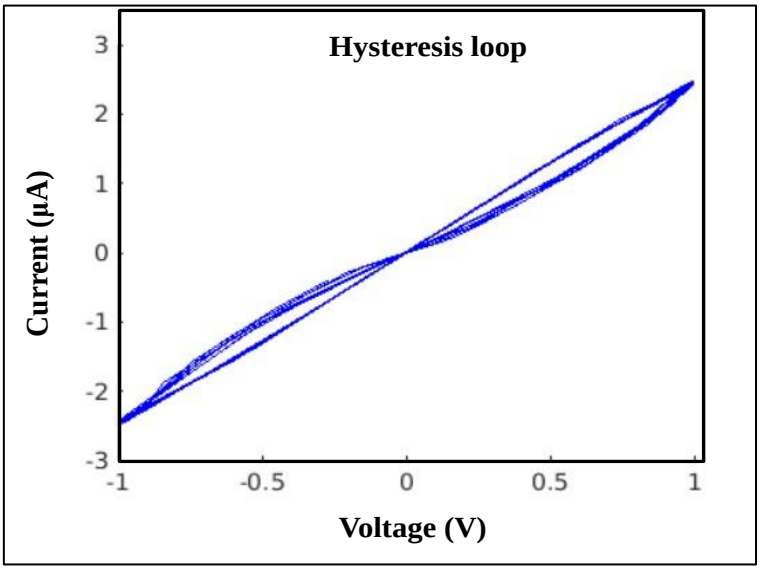

Figure 8. Hysteresis loop of the sensing element

From the result, it can be seen that the hysteresis loop is passing through the origin and hence it shows the memristor properties. The pinched hysteresis loop is the confirmatory nature of a memristor, which shows that the resistance of the element changes from R_{off} to a higher value R_{on} when exposed to 3-Carene. The loop area of the hysteresis loop obtained for the nanocomposite understudy is narrow, but the sensitivity of the nanocomposite, when used as a sensor, depends on the ratio $(R_{on}-R_{off})/R_{off}$ and it is independent of the hysteresis loop area [33]. On exposure to the VOC along with the alternating current source of frequency 5 rad/s, the variations in relative depth of the gas occupied sensing area obtained through simulations is shown in Figure 9. Since the nanocomposite is having a porous sheet structure, the penetration of target VOC is comparatively higher.

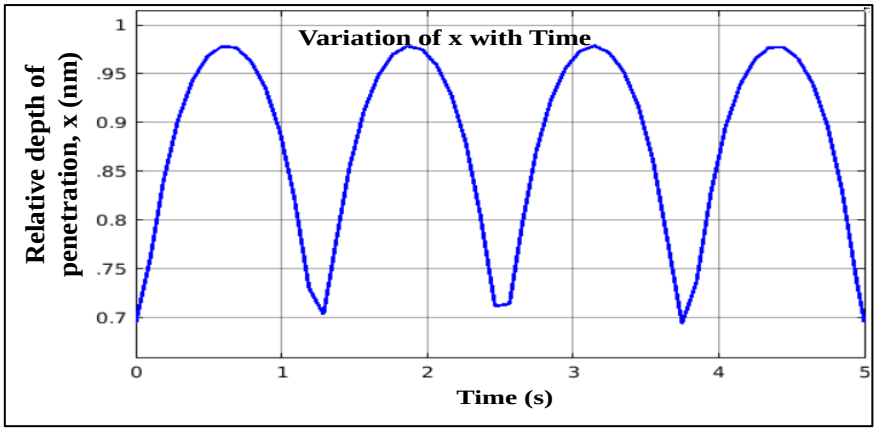

Figure 9. Relative depth variation of the VOC occupied sensing area

4. CONCLUSION

The impedance measurement of the polyaniline-WO_3 nanocomposite with a frequency variation from 100Hz to 5MHz at room temperature was performed. The impedance spectroscopy analysis using a Nyquist plot showed that the major conduction mechanism in the synthesized nanocomposite as a grain boundary effect. The depressed semicircle Nyquist plot of the polyaniline-WO_3 nanocomposite shows that the material obeys a non-Debye model of relaxation mechanism. The equivalent circuit model for 5, 10, 15 and 20 weight percentage of polyaniline-WO_3 nanocomposites were simulated and their equivalent circuit parameters were calculated. The grain boundary parameters of the synthesized polyaniline-WO_3 nanocomposites were computed and nanocomposite with a WO_3 doping concentration of 15% exhibited a lower grain boundary resistance compared to all the other nanocomposites prepared in this work. The average crystallite size for the synthesized nanocomposites was calculated from the XRD results. The sharp peaks in the X-ray diffractogram confirmed the monoclinic crystal structure of WO_3 nanoparticles in the nanocomposite. The FESEM images show the sheet structure of polyaniline nanocomposite with 15% of WO_3 doping concentration. The memristor sensor model of the polyaniline nanocomposite doped with 15% of WO_3 was simulated using MATLAB-Simulink using Joglekar's window function. The memristor studies were conducted to investigate the room temperature VOC sensing characteristics of polyaniline-WO_3 nanocomposite with 15% doping concentration towards the target VOC, 3-Carene which is a breath-based biomarker for malaria. The pinched hysteresis loop obtained in the simulation results confirmed the memristor properties of the material and voltage and current were found to be in phase with each other. The results suggest that polyaniline-WO_3 nanocomposite with 15% doping concentration can be used for the fabrication of a chemiresistive VOC sensor for the detection of 3-Carene, the breath-based biomarker for malaria at room temperature.

ACKNOWLEDGEMENTS

The authors would like to acknowledge Polymer Composites Research Lab and Centre of Excellence on Advanced Material Research Lab of B.M.S. College of Engineering, Bangalore for providing the research facilities.

REFERENCES

[1] L. Chua, "Memristor-The Missing Circuit Element," *IEEE Trans. circuit theory*, vol. CT-18, no. 5, pp. 507–519, 1971.

[2] D. B. Strukov, G. S. Snider, D. R. Stewart, and R. S. Williams, "The missing memristor found," *Nature*,

vol. 453, no. 7191, pp. 80–83, 2008, doi: 10.1038/nature06932.
[3] J. J. Yang, M. D. Pickett, X. Li, D. A. A. Ohlberg, D. R. Stewart, and R. S. Williams, "Memristive switching mechanism for metal/oxide/metal nanodevices," *Nat. Nanotechnol.*, vol. 3, no. 7, pp. 429–433, 2008, doi: 10.1038/nnano.2008.160.
[4] R. Waser and M. Aono, "Nanoionics-based resistive switching memories," *Nanosci. Technol. A Collect. Rev. from Nat. Journals*, pp. 158–165, 2009, doi: 10.1142/9789814287005_0016.
[5] V. Erokhin and M. P. Fontana, "Thin film electrochemical memristive systems for bio-inspired computation," *J. Comput. Theor. Nanosci.*, vol. 8, no. 3, pp. 313–330, 2011, doi: 10.1166/jctn.2011.1695.
[6] V. Erokhin, T. Berzina, and M. P. Fontana, "Hybrid electronic device based on polyaniline-polyethyleneoxide junction," *J. Appl. Phys.*, vol. 97, no. 6, 2005, doi: 10.1063/1.1861508.
[7] Q. Wang, Y. Z. Pan, S. S. Huang, S. T. Ren, P. Li, and J. J. Li, "Resistive and capacitive response of nitrogen-doped TiO2 nanotubes film humidity sensor," *Nanotechnology*, vol. 22, no. 2, 2011, doi: 10.1088/0957-4484/22/2/025501.
[8] S. Carrara, D. Sacchetto, M. A. Doucey, C. Baj-Rossi, G. De Micheli, and Y. Leblebici, "Memristive-biosensors: A new detection method by using nanofabricated memristors," *Sensors Actuators, B Chem.*, vol. 171–172, pp. 449–457, 2012, doi: 10.1016/j.snb.2012.04.089.
[9] A. A. Haidry, A. Ebach-Stahl, and B. Saruhan, "Effect of Pt/TiO2 interface on room temperature hydrogen sensing performance of memristor type Pt/TiO2/Pt structure," *Sensors Actuators, B Chem.*, vol. 253, pp. 1043–1054, 2017, doi: 10.1016/j.snb.2017.06.159.
[10] D. E. Williams, G. S. Henshaw, K. F. E. Pratt, and R. Peat, "Reaction-diffusion effects and systematic design of gas-sensitive resistors based on semiconducting oxides," *J. Chem. Soc. Faraday Trans.*, vol. 91, no. 23, pp. 4299–4307, 1995, doi: 10.1039/FT9959104299.
[11] H. Abunahla *et al.*, "MemSens: Memristor-Based Radiation Sensor," *IEEE Sens. J.*, vol. 18, no. 8, pp. 3198–3205, 2018, doi: 10.1109/JSEN.2018.2808285.
[12] C. Zhang *et al.*, "Bioinspired Artificial Sensory Nerve Based on Nafion Memristor," *Adv. Funct. Mater.*, vol. 29, no. 20, pp. 1–10, 2019, doi: 10.1002/adfm.201808783.
[13] S. Abdul Hadi, K. M. Humood, M. Abi Jaoude, H. Abunahla, H. F. Al Shehhi, and B. Mohammad, "Bipolar Cu/HfO2/p++ Si Memristors by Sol-Gel Spin Coating Method and Their Application to Environmental Sensing," *Sci. Rep.*, vol. 9, no. 1, pp. 1–15, 2019, doi: 10.1038/s41598-019-46443-x.
[14] D. A. Lapkin *et al.*, "Polyaniline-based memristive microdevice with high switching rate and endurance," *Appl. Phys. Lett.*, vol. 112, no. 4, 2018, doi: 10.1063/1.5013929.
[15] K. K. Gogoi and A. Chowdhury, "Electric field induced tunable memristive characteristics of exfoliated graphene oxide embedded polymer nanocomposites," *J. Appl. Phys.*, vol. 126, no. 2, 2019, doi: 10.1063/1.5102145.
[16] K. Gorshkov, T. Berzina, V. Erokhin, and M. P. Fontana, "Organic memristor based on the composite materials: Conducting and ionic polymers, gold nanoparticles and graphenes," *Procedia Comput. Sci.*, vol. 7, pp. 248–249, 2011, doi: 10.1016/j.procs.2011.09.020.
[17] T. D. Dongale *et al.*, "Development of Ag/WO3/ITO thin film memristor using spray pyrolysis method," *Electron. Mater. Lett.*, vol. 11, no. 6, pp. 944–948, 2015, doi: 10.1007/s13391-015-4180-4.
[18] L. Chua, "Resistance switching memories are memristors," *Appl. Phys. A Mater. Sci. Process.*, vol. 102, no. 4, pp. 765–783, 2011, doi: 10.1007/s00339-011-6264-9.
[19] S. F. Abdullah, S. Radiman, M. A. A. Hamid, and N. B. Ibrahim, "Studies on the phase transitions and properties of tungsten (VI) oxide nanoparticles by X-Ray diffraction (XRD) and thermal analysis," *ASEAN J. Sci. Technol. Dev.*, vol. 26, no. 1, pp. 13–20, 2017, doi: 10.29037/ajstd.300.
[20] P. Jisha, M. S. Suma, and M. V. Murugendrappa, "Synthesis and characterization of WO3-doped polyaniline to sense biomarker VOCs of Malaria," *Appl. Nanosci.*, 2020, doi: 10.1007/s13204-020-01551-3.
[21] B. K. Money and J. Swenson, "Dynamics of poly(ethylene oxide) around its melting temperature," *Macromolecules*, vol. 46, no. 17, pp. 6949–6954, 2013, doi: 10.1021/ma4003598.
[22] B. J. T. S. Irvine, D. C. Sinclair, and A. R. West, "<Electroceramics Characterisation by impedance sepctroscopy.pdf>," vol. 2, no. 3, pp. 132–138, 1990.
[23] K. S. Hemalatha, G. Sriprakash, M. V. N. Ambika Prasad, R. Damle, and K. Rukmani, "Temperature dependent dielectric and conductivity studies of polyvinyl alcohol-ZnO nanocomposite films by impedance spectroscopy," *J. Appl. Phys.*, vol. 118, no. 15, 2015, doi: 10.1063/1.4933286.
[24] P. Jisha, M. S. Suma, M. V. Murugendrappa, and K. Raj, "A study on the effect of PVDF on the structural and transport properties of polyaniline," *Int. J. Polym. Anal. Charact.*, vol. 25, no. 4, pp. 176–187, 2020, doi: 10.1080/1023666X.2020.1779431.

[25] M. R. Shoar Abouzari, F. Berkemeier, G. Schmitz, and D. Wilmer, "On the physical interpretation of constant phase elements," *Solid State Ionics*, vol. 180, no. 14–16, pp. 922–927, 2009, doi: 10.1016/j.ssi.2009.04.002.

[26] M. Sowa and W. Simka, "Electrochemical impedance and polarization corrosion studies of tantalum surface modified by DC Plasma electrolytic oxidation," *Materials (Basel).*, vol. 11, no. 4, 2018, doi: 10.3390/ma11040545.

[27] A. Gupta and J. Sakamoto, "Controlling Ionic Transport through the PEO-LiTFSI/LLZTO Interface," *Electrochem. Soc. Interface*, vol. 28, no. 2, pp. 63–69, Jul. 2019, doi: 10.1149/2.F06192if.

[28] J. Jose and M. Abdul Khadar, "Role of grain boundaries on the electrical conductivity of nanophase zinc oxide," *Mater. Sci. Eng. A*, vol. 304–306, no. 1–2, pp. 810–813, 2001, doi: 10.1016/S0921-5093(00)01579-3.

[29] Hashemi Karouei, S., Milani Moghaddam, H. & Saadat Niavol, S, "Characterization and gas sensing properties of graphene/polyaniline nanocomposite with long-term stability under high humidity", *J Mater Sci* , Vol. 56, pp. 4239–4253, 2021, doi: 10.1007/s10853-020-05532-3.

[30] Jisha, P., Suma, M.S., Murugendrappa, M.V. et al, "Fabrication, characterization, and malaria biomarker VOC-sensing properties of WO3-doped polyaniline", *J Mater Sci: Mater Electron*, Vol. 32, pp.11243–11263, March 2021, doi:10.1007/s10854-021-05794-w

[31] K. Zaplatilek and C. Republic, "Memristor modeling in MATLAB ® &Simulink ®," *Differ. Equations*, pp. 62–67, 2008.

[32] E. Apollos, "Memristor Theory and Mathematical Modelling," *Int. J. Comput. Appl.*, vol. 178, no. 27, pp. 1–8, 2019, doi: 10.5120/ijca2019919089.

[33] N. S. Mohamad Hadis, A. Abd Manaf, S. H. Ngalim, and S. H. Herman, "Fabrication and characterisation of fluidic based memristor sensor for liquid with hydroxyl group," *Sens. Bio-Sensing Res.*, vol. 14, no. April, pp. 21–29, 2017, doi: 10.1016/j.sbsr.2017.04.002.